Marine Biotechnology (2024) 26:790–809
https://doi.org/10.1007/s10126-024-10347-3

RESEARCH

Multiomics Analyses Explore the Immunometabolic Interplay in the Liver of White Crucian Carp (*Carassius cuvieri*) After *Aeromonas veronii* Challenge

Fei Wang[1] · Zi-Rou Zhong[1] · Qing Xie[1] · Jie Ou[1] · Ning-Xia Xiong[2] · Ming-Zhu Huang[3] · Shi-Yun Li[1] · Gang Hu[1] · Zi-Le Qin[1] · Sheng-Wei Luo[1]

Received: 13 May 2024 / Accepted: 13 July 2024 / Published online: 23 July 2024

Abstract

Aeromonas veronii is one of the predominant pathogenic species that can imperil the survival of farmed fish. However, the interactive networks of immune regulation and metabolic response in *A. veronii*–infected fish are still unclear. In this investigation, we aimed to explore immunometabolic interplay in white crucian carp (WCC) after the *A. veronii* challenge. Elevated levels of immune-related genes were observed in various tissues after *A. veronii* infection, along with the sharp alteration of disease-related enzymatic activities. Besides, decreased levels of antioxidant status were observed in the liver, but most metabolic gene expressions increased dramatically. Multiomics analyses revealed that metabolic products of amino acids, such as formiminoglutamic acid (FIGLU), L-glutamate (L-Glu), and 4-hydroxyhippuric acid, were considered the crucial liver biomarkers in *A. veronii*–infected WCC. In addition, *A. veronii* infection may dysregulate endoplasmic reticulum (ER) function to affect the metabolic process of lipids, carbohydrates, and amino acids in the liver of WCC. These results may have a comprehensive implication for understanding immunometabolic response in WCC upon *A. veronii* infection.

Keywords Crucian carp · Immunometabolism · *Aeromonas veronii* · Oxidative damage

Introduction

Teleost fish possessed a large quantity of immune-related factors, including pathogen-recognizing clusters, but environmental stressors and invasive pathogens may cause physiological disorder and immune suppression (Stoliar and Lushchak 2012; Magnadottir 2010). Crucian carp (*Carassius auratus*) is one of the popular cultivated fish species in China, but it frequently suffers from various infectious diseases (Li et al. 2018). Recent findings indicate that some invasive pathogens can evade host immunity by suppressing microbicidal response, which may enable them to survive and proliferate within the host (Bernard et al. 2018). Following succeeding in the breach of mucosal epithelial barriers, invading pathogens can deepen infection processes in inflammatory foci (Secombes et al. 2001). The liver is a frontline immune organ receiving gut-derived substances to confer protection against circulating antigens and foreign endotoxins (Xiong et al. 2023). Besides, the liver is a predominant site associated with immune defense by generating 80 to 90% of complement components and pattern-recognition receptors, which plays a pivotal role in detoxification, metabolic processes, and immune surveillance (Bols et al. 2001; Wu et al. 2016). Our previous study indicated that inflammatory cytokine could dysregulate mucosal immunity and then aggravate *Aeromonas hydrophila*–induced injury in the gut-liver axis of crucian carp (Xiong et al. 2023; Li et al. 2024). *Aeromonas veronii*, one of the predominant species in *Aeromonas* genus, can lead to infected fish suffering from hemorrhagic septicemia, bilateral exophthalmia, and

✉ Sheng-Wei Luo
swluo@hunnu.edu.cn; swluo1@163.com

[1] State Key Laboratory of Developmental Biology of Freshwater Fish, Engineering Research Center of Polyploidy Fish Reproduction and Breeding of the State Education Ministry, College of Life Science, Hunan Normal University, Changsha 410081, People's Republic of China

[2] Department of Aquatic Animal Medicine, College of Fisheries, Huazhong Agricultural University, Wuhan 430070, People's Republic of China

[3] National R&D Center for Freshwater Fish Processing, Jiangxi Normal University, Nanchang 330022, China

ocular disorders, which may cause a great economic loss in aquaculture (Ibrahim et al. 2024).

The transcriptomic analysis is able to offer a deep understanding of complex signal pathways with the real-time monitoring of gene expressions (Maekawa et al. 2019), whereas metabolome is a systemic biology that characterizes the alteration of endogenous metabolites involved in various biological processes, including lipid synthesis, glucose metabolism and mitochondrial ability (Yang et al. 2023). To date, single-omics studies cannot comprehensively account for the underlying pathogenesis of particular diseases; thus, the application of multiomics research is urgently required (Chen et al. 2023). Immunometabolism is an emerging field of investigation linking immunology to metabolism, which can provide a novel insight into the mechanism between infection-induced symptoms and innate/adaptive immune regulation (Lercher et al. 2020). However, the metabolic and redox response of white crucian carp (WCC, *Carassius cuvieri*) following *A. veronii* infection is still unclear.

In this study, the aims were to evaluate pathological features and antioxidant status in WCC following *A. veronii* infection. Following that, an integrated investigation of transcriptome and metabolome was performed for a comprehensive understanding of immunometabolic interplay in *A. veronii*–infected fish.

Materials and Methods

Animal Preparation and Experimental Design

Healthy WCCs (about 19.24 ± 0.78 g) were collected from a fishing base in Wangcheng district, Changsha, China. Fish were daily fed with commercial crucian carp diets (2 mm, Tongwei Co., Ltd., China) for a 2-week acclimation in clean circulating water (21–24 °C, pH 7.6–8.2) till 24 h before the infection experiment. Fish feed and feces were removed daily to avoid pathogenic contamination during fish acclimation and infection periods.

The diagram of the experimental step is shown in Fig. S1. To investigate immunometabolic interplay in *A. veronii*–infected WCCs, a total of 50 fish were randomly divided and sacrificed for tissue section, bacterial loads, biochemistry analyses, and multiomics analyses. In brief, *A. veronii* G2-2 was isolated from a dying cyprinid fish and subjected to 16S rRNA sequencing (accession number, OM190459). The detailed information about strain G2-2 is presented in Table 1. Strain G2-2 was cultured in Luria–Bertani (LB) medium at 28 °C for 24 h and resuspended in PBS (phosphate-buffered saline, pH 7.3) before the infection process. Fish infected with 100 μL suspension of 1×10^7 CFU mL^{-1} *A. veronii* in PBS was used as the infection group (WCCLAv), while injection of 100 μL sterile PBS was used as the control group (WCCLCtl). Liver samples were isolated from WCC at 24 h post-infection.

DNA Preparation for Bacterial Load Detection

To investigate the effect of *A. veronii* infection on tissue injury, a bacterial load assay was performed (Wang et al. 2017). In brief, genomic DNA was extracted from the isolated tissues (liver, kidney, spleen, and intestine) by using a tissue DNA extraction kit (Magen Biotechnology, China). Before detection, DNA concentration was adjusted to 100 ng/μL before use.

Determination of Biochemical Activity

The above isolated tissues (liver, kidney, spleen, and intestine) were homogenized in ice-cold 1 × PBS buffer. Following centrifugation at 10,000 × g for 10 min at 4 °C, the supernatants were quantified by using the bicinchoninic acid (BCA) method.

For measurement of disease-related indexes, supernatants of tissue homogenates were used to detect alkaline phosphatase (AKP) activity, aspartate aminotransferase (AST) activity, alanine aminotransferase (ALT) activity, and acid phosphatase (ACP) activity, respectively. According to the manufacturer's instructions, AKP activity was measured at OD_{520} nm by using a AKP kit (Nanjing Jiancheng Bioengineering Institute, China). AST activity was measured at OD_{510} nm by using a AST kit (Nanjing Jiancheng Bioengineering Institute, China). ALT activity was measured at OD_{510} nm by using a ALT kit (Nanjing Jiancheng Bioengineering Institute, China). ACP activity was measured at OD_{520} nm by using a ACP kit (Nanjing Jiancheng Bioengineering Institute, China).

Table 1 Detail information of *Aeromonas veronii* G2-2

Strain name	G2-2
Accession number	OM190459
Pathogenic isolation	Strain G2-2 was isolated from the gill of a dying cyprinid fish
Virulence gene	Strain G2-2 contains aerA gene
Culture medium	Luria–Bertani medium
Susceptibility	Most freshwater fish, including crucian carp and grass carp
Pathological feature	Abdominal swelling and skin congestion

For measurement of antioxidant indexes, liver supernatant was used to detect catalase (CAT) activity, glutathione peroxidase (GPx) activity, glutathione reductase (GR) activity, lactate dehydrogenase (LDH) activity, monoamine oxidase (MAO) activity, and succinate dehydrogenase (SDH) activity. Liver CAT activity was detected at OD_{405} nm by using a CAT kit (Nanjing Jiancheng Bioengineering Institute, China). Liver GPx activity was detected at OD_{340} nm by using a GPx kit (Beyotime Biotechnology, China). Liver GR activity was detected at OD_{412} nm by using a GR kit (Nanjing Jiancheng Bioengineering Institute, Nanjing, China). Liver LDH activity was detected at OD_{490} nm by using a LDH kit (Beyotime Biotechnology, China). Liver MAO activity was detected at OD_{242} nm by using a MAO kit (Nanjing Jiancheng Bioengineering Institute, China). Liver SDH activity was detected at OD_{600} nm by using a SDH kit (Nanjing Jiancheng Bioengineering Institute, China). The calculated results were subjected to triplicate measurements.

Pathological Section Analysis

Liver samples were fixed in the Bouin solution. Then, fixed samples were paraffin-embedded and prepared for tissue slices (5-μm-thick) by using a Paraffin slicing machine (Leica RM2235). According to the manufacturer's instructions, tissue slices were stained by using a hematoxylin and eosin (HE) staining kit (Xiong et al. 2022). Then, pathological sections were observed by using a light microscope (Leica DM 4000 with Leica Q Vin 3 program) with 200 × magnification. The experiment was repeated in triplicate.

Metabolite Features and Functional Annotation by LC–MS/MS

Metabolomics analysis was performed as previously described (Lu et al. 2008). In brief, liver tissues isolated from WCC were homogenized in ice-cold 1 × PBS buffer, and then filtrated samples were dried in a vacuum. Metabolic analysis was performed by using UPLC coupled to QTOF-MS in both positive and negative ion mode along with quality controls throughout the experimental run. Each group contained six independent samples for biological repeats.

Raw data were calculated by the XCMS program. Following that, filtered data were shown with retention time (RT), ratio of mass/charge (m/z), and coefficient of variation (CV). After identification by the metabolome database, metabolic results were validated by PLS-DA and OPLS-DA models. The threshold of differential metabolite (DM) rank was set as below: variable importance in projection (VIP) ≥ 1, p-value < 0.05, and fold change (FC) > 1.5 or < 0.667. Then, DM contents were presented by heatmap analysis. Metabolic proximities of DMs were analyzed by Pearson correlation analysis. According to VIP values, the data distribution and probability density of crucial DMs were evaluated. Then, metabolic pathways of crucial DMs were determined by the Kyoto Encyclopedia of Genes and Genomes (KEGG) database. The changed levels of DMs in KEGG pathways were calculated by differential abundance (DA) score.

RNA-seq Assemble and Functional Annotation

Total RNA was isolated from liver samples by using an RNeasy Kit (Qiagen, Germany). Total RNA (RIN > 7.0, OD260/280 = 2.0 to 2.2) was enriched from each sample for cDNA construction and purified for PCR amplification by using the Illumina HiSeq platform. Following that, clean reads with high quality were obtained after the removal of raw reads possessing adapter contaminants, reads with more than 10% *N* and low-quality reads. Obtained clean reads were mapped to reference the genome of red crucian carp (*Carassius auratus* red variety) by HISAT software. Based on FPKM values and principal component analysis (PCA), expressions of differentially expressed genes (DEGs) were quantified by DESeq2 software. Then, expression patterns of DEGs were evaluated by using K-means clustering analysis. Then, functional annotation of DEG was performed by gene ontology (GO) and the Kyoto Encyclopedia of Genes and Genomes (KEGG).

Joint Analyses of Multiomics Results

The integrated analyses of transcriptomic and metabolomics results were validated by the O2PLS model. The threshold of correlation analysis between DEGs and DMs was set as below: coefficient value > 0.8 or < −0.8, p-value < 0.05. The relations between DEGs and DMs were calculated by canonical correlation analysis (CCA). The coexpression patterns of DEGs and DMs were analyzed by nine quadrant plot and correlation clustering heatmap, respectively. Then, the functional annotation of DEGs and DMs was calculated by KEGG analysis. The correlation network diagram was conducted by Cytoscape and Visio software.

RNA Extraction and cDNA Synthesis

In order to validate the immune regulation and metabolic response in WCC following *A. veronii* infection, expressions of crucial genes were analyzed by qRT-PCR assay, and qRT-PCR results were subjected to melting curve analysis (Qi et al. 2011). In brief, total RNA was extracted from isolated tissues (liver, kidney, spleen, and intestine) and treated with

DNAase to avoid genomic DNA contamination by using FastPure cell/tissue Total RNA isolation Kit v2 (Vazyme Biotech, China) (Li et al. 2024). After RNA quality confirmation, 1000 ng of purified total RNA was used for cDNA synthesis by using MonScript™ RT III All-in-One Mix with dsNase (Monad, China).

Quantitative Real-Time PCR (qRT-PCR) Assay

Relative levels of *A. veronii* virulent genes and immunometabolic genes were evaluated by qRT-PCR assay. For bacterial loads, relative expression of *A. veronii aerA* gene was detected in the liver, kidney, spleen, and intestine, while *GAPDH* was used as a reference gene. For analysis of pathological response, relative expression levels of cluster of differentiation 3 (*CD3*), cluster of differentiation 4 (*CD4*), lysozyme C (*lysC*), insulin-like growth factor (*IGF*), heat shock protein 70 (*HSP70*), apolipoprotein D (*ApoD*), and major histocompatibility complex-I (*MHC-I*) were analyzed in the liver, kidney, spleen, and intestine. For validation of transcriptome and metabolome, relative expression profiles of diacylglycerol acyltransferase 2 (*DGAT2*), nucleoside diphosphate kinase A (*NDPK-A*), peroxisome proliferator-activated receptor gamma (*PPARγ*), lipocalin (*LIPO*), cyclic AMP-responsive element binding protein 3 (*CREB3*), fatty acid transport protein 1 (*FATP1*), fatty acid transport protein 4 (*FATP4*), coenzyme Q-binding protein COQ10 homolog (*COQ10*), cell cycle checkpoint protein RAD1 (*RAD1*), warm temperature acclimation related 65 kDa protein-1 (*WAP65-1*), mannose-binding protein C (*MBP-C*), tumor necrosis factor receptor superfamily member 11A (*TNFRSF11A*), p53-binding protein 2 (*p53BP2*), complement factor I (*CFI*), E3 ubiquitin-protein ligase TRIM39 (*TRIM39*), and complement factor B (*CFB*) were investigated in the liver. 18S rRNA was used as a reference gene. After triplicate detection, qRT-PCR results were calculated by $2^{-\Delta\Delta Ct}$ method. The primers are shown in Table 2. Additionally, the qRT-PCR reaction contained 10.0 µL SYBR Green Master Mix (ABI), 2.0 µL DNA/cDNA template, 0.5 µL each primer, and 7.0 µL ddH_2O. The program contained 1 cycle of 95 °C for 30 s, 40 cycles of 95 °C for 15 s, 60 °C for 35 s, followed by 1 cycle of 95 °C for 30 s, and 60 °C for 60 s. At the end of qRT-PCR amplified reactions, the melting curve analysis was implemented to confirm the credibility of each qRT-PCR analysis.

Statistical Analyses

The qRT-PCR results and enzymatic activities in tissues were subjected to *T*-test analysis by using SPSS 17.0 software. If the analytical levels reach less than 0.05 *p*-value, results were statistically significant.

Table 2 The primer sequences used in this study

Primer names	Sequence direction (5′→3′)	Use
RT-18S-F	CGGAGGTTCGAAGACGATCA	qPCR
RT-18S-R	GAGGTTTCCCGTGTTGAGTC	qPCR
RT-DGAT2-F	TTCAGCACAGACCGTAATGGA	qPCR
RT-DGAT2-R	TAGGCACAGTAATGGGACCG	qPCR
RT-NDPK-A-F	AGCGAGATTTGCTCTGTGCG	qPCR
RT-NDPK-A-R	CAGGCTGGCGTAGAAGGGTT	qPCR
RT-COQ10-F	AGAGCCGAAGCATTGGTTACT	qPCR
RT-COQ10-R	TGATTGAAGAGCATCCCGTC	qPCR
RT-PPARγ-F	GAAGCCGTCAGCGAAGTCA	qPCR
RT-PPARγ-R	ATCATTTCACAGAAGGGTTTGC	qPCR
RT-LIPO-F	GATGCTGTGCGTTCTGCTCT	qPCR
RT-LIPO-R	CCTTCCTTGGTCTTGATGGTG	qPCR
RT-CREB3-F	TCACTGATGGAACAACTGCGT	qPCR
RT-CREB3-R	GGGAGTATTTTGGAGTCGTCTG	qPCR
RT-FATP1-F	AACAGTCGCATTCTGCCAAA	qPCR
RT-FATP1-R	GCTCGTCCATAACTAAAACATCAC	qPCR
RT-FATP4-F	GATGTGCTGGAGATGGACGA	qPCR
RT-FATP4-R	CCTGAGACGATGCTGCGAT	qPCR
RT-gapdh-F	CAGGGTGGTGCCAAGCG	qPCR
RT-gapdh-R	GGGGAGCCAAGCAGTTAGTG	qPCR
RT-aerA-F	CCTATGGCCTGAGCGAGAAG	qPCR
RT-aerA-R	CCAGTTCCAGTCCCACCACT	qPCR
RT-ApoD-F	GCTTCATTGAGGGAACTGCC	qPCR
RT-ApoD-R	GGGATTTGAGGATGCCTAACA	qPCR
RT-CD3-F	ATGAGTTGAGCAGGCTGAGGG	qPCR
RT-CD3-R	AGGGTTCGCTGGTTTGGGA	qPCR
RT-CD4-F	GATTGCTGTAGGAGCCAGTTCT	qPCR
RT-CD4-R	ACCCTCTTCTTCATCCGTTTG	qPCR
RT-HSP70-F	ACGAGGCAGTGGCTTATGG	qPCR
RT-HSP70-R	GGGTCTGTTTGGTGGGGAT	qPCR
RT-IGF-F	ATGAAGGACCACAAAAGCCC	qPCR
RT-IGF-R	TCGCCAAAATCTCCACTGC	qPCR
RT-lysC-F	ATGAAGGTGGCGATTGCG	qPCR
RT-lysC-R	AAACTTGCTTTCCCAGTAGGC	qPCR
RT-MHC-1-F	CAGGTCGCAATGAAACGCT	qPCR
RT-MHC-1-R	GCTGGTCTTCTGAAAGGTCCC	qPCR
RT-TRIM39-F	GCTAAACAACGCACCTGGAA	qPCR
RT-TRIM39-R	ATCAAATCGCTGAGGGCTG	qPCR
RT-CFI-F	CAACGGACAGCATCCCAGT	qPCR
RT-CFI-R	CGTCACATTTGCCCATTTTAG	qPCR
RT-p53BP2-F	GTGAACGCCGCCGACA	qPCR
RT-p53BP2-R	GGACGCCGTAGAGGAACTGA	qPCR
RT-TNFRSF11A-F	CGAACCCCGCCAGAGTC	qPCR
RT-TNFRSF11A-R	GCCAGAAGGGCTGCTGTAGT	qPCR
RT-MBP-C-F	CTTATGGAGTTTGTGCCGCTAC	qPCR
RT-MBP-C-R	TCCCGCTTTCCTGAATGTG	qPCR
RT-Wap65-1-F	GCACTGGAGCCTTCCGTTA	qPCR
RT-Wap65-1-R	CCTTCAGGGGTTTGGGGTA	qPCR
RT-RAD1-F	AACATCCTGAAAGCCATCTCC	qPCR
RT-RAD1-R	AGCACATTCTCAAGGCGGTA	qPCR

Table 2 (continued)

Primer names	Sequence direction (5′→3′)	Use
RT-CFB-F	GCAAAGACCAACCCTATCGG	qPCR
RT-CFB-R	TCCCTCTGTGACACTAAGCCAT	qPCR

Results

Determination of Pathological Response in Tissues

In Fig. 1A, 62.1-, 2.7-, 3.5- and 15.5-fold increased expressions of *aerA* gene were detected in the liver, kidney, spleen, and intestine following *A. veronii* challenge.

Seven immunometabolic genes were selected for expression analysis following *A. veronii* challenge (Fig. 1B). Relative expressions of *ApoD* and *MHC-I* were higher than that of other detected genes. The highest expression of *ApoD* was observed in the intestine, followed by the kidney, while the expression of liver *MHC-I* increased sharply with the highest value ($p < 0.05$). Four crucial disease-related enzymatic activities were measured in isolated tissues (Fig. S2). In Fig. 1C, ALT activities increased by 2.1-, 3.9-, 6.9- and 2.5-fold in the liver, kidney, spleen, and intestine of WCC following *A. veronii* challenge ($p < 0.05$). A 2.5- and 2.7-fold increase in AST activities were detected in the spleen and intestine of WCC after the *A. veronii* challenge, while AST activities in the liver and kidney decreased sharply ($p < 0.05$). A 1.6- and 1.4-fold increase in ACP activities was detected in the liver and kidney following *A. veronii* challenge, while ACP activities in the spleen and intestine declined sharply ($p < 0.05$). A 1.8-, 1.4- and 1.5-fold increase in AKP activities was observed in the liver, spleen, and intestine following *A. veronii* challenge, while AKP activity in the kidney decreased sharply ($p < 0.05$).

Evaluation of Tissue Damage and Oxidative Status in the Liver

As shown in Fig. 2A, B, a marked morphological change was detected in the liver of WCC after *A. veronii* challenge. *A. veronii* infection could stimulate ranges of tissue damage in the liver of WCC, including nuclear vanish, cell swelling, and cell boundary blurring.

Antioxidant parameters in the liver following *A. veronii* challenge is shown in Fig. 2. In Fig. 2C–H, 2.73-, 1.20-, 1.39-, 1.42- and 1.48-fold decrease in CAT, GPx, GR, MAO, and SDH activity was detected in the liver of WCC following *A. veronii* challenge, along with an increased level of LDH activity ($p < 0.05$).

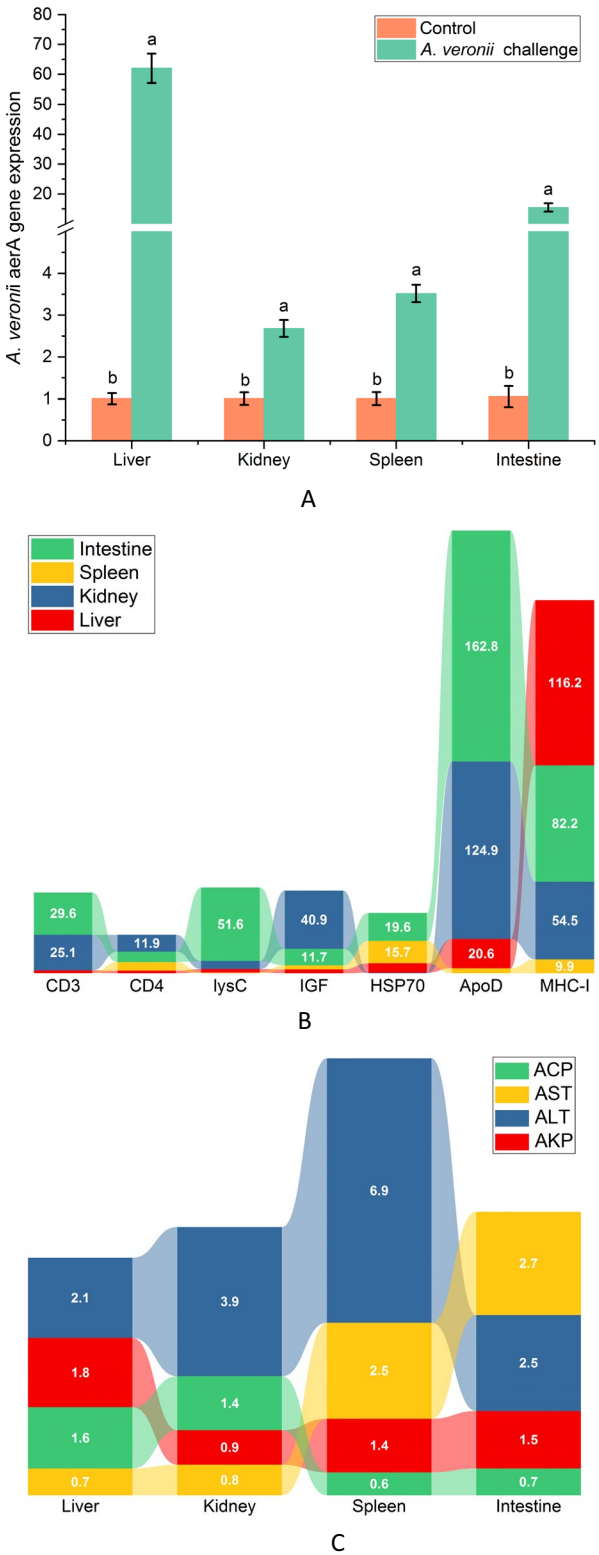

Fig. 1 Measurement of pathological response in WCC following *A. veronii* challenge. **A** Detection of *A. veronii* aerA gene expression in isolated tissues. **B** Crucial gene expressions in the liver, kidney, spleen, and intestine. **C** Ratios of disease-related enzymatic activities in the liver, kidney, spleen, and intestine. The calculated data (mean ± SD) with different letters were significantly different ($p < 0.05$)

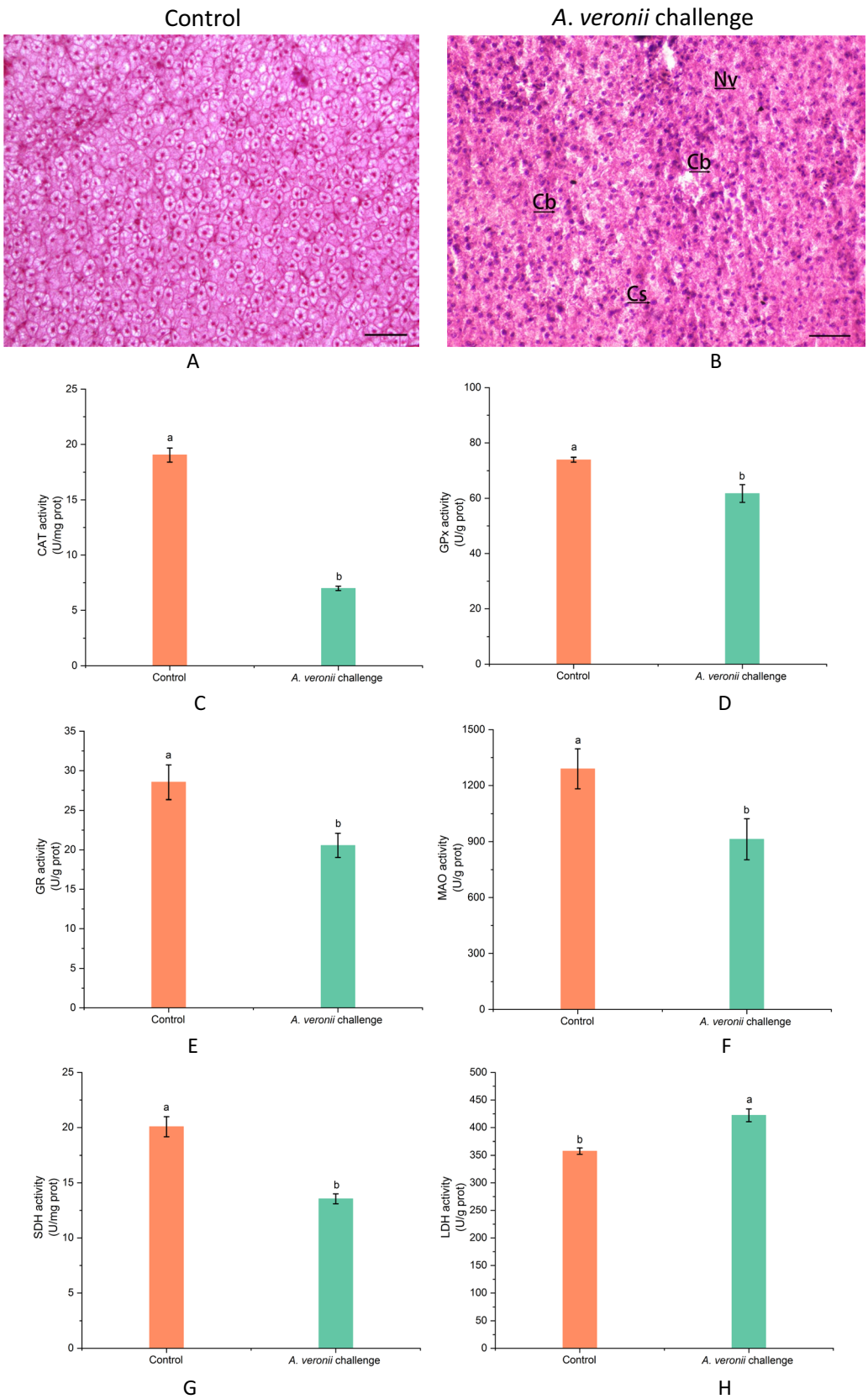
Control
A. veronii challenge
Nv
Cb
Cb
Cs
A
B
CAT activity (U/mg prot)
GPx activity (U/g prot)
Control
A. veronii challenge
C
D
GR activity (U/g prot)
MAO activity (U/g prot)
E
F
SDH activity (U/mg prot)
LDH activity (U/g prot)
G
H

◂**Fig. 2** Histological section and antioxidant status in the liver of WCC following *A. veronii* challenge. **A**, **B** Liver histological observation. The control samples and *A. veronii*–infected samples were sectioned and stained by using a hematoxylin and eosin (HE) staining kit. Nv, nuclear vanish; Cb, cell boundary blurring; Cs, cell swelling. **C**–**H** Antioxidant status in the liver of WCC. CAT, GPx, GR, MAO, SDH, and LDH were measured by microplate methods. The calculated data (mean ± SD) with different letters were significantly different ($p < 0.05$)

Liver Metabolic Features Following *A. veronii* Challenge

To characterize key metabolic biomarkers in WCC after the *A. veronii* challenge, a total of 2457 metabolites were mapped to metabolomics databases. In Fig. 3A, "Benzene and substituted derivatives" showed the highest proportion (17.13%) in the metabolic category. Formiminoglutamic acid (FIGLU) presented the highest content in obtained metabolic results, followed by ethylene oxide, methylsuccinic acid, and D-ribofuranose 5-phosphate, whereas acrylamide was found to be the lowest content of metabolite (Fig. 3B). The clear separation of metabolic features was subjected to PLS-DA and OPLS-DA models (Fig. S3A-D). Based on the OPLS-DA model, S plot analysis was implemented to confirm the DM differentiation by calculation of the VIP threshold in metabolome (Fig. S3E). In Fig. S3F, a total of 240 DMs were observed in the liver of WCC after *A. veronii* infection, possessing 205 increased metabolites and 35 decreased metabolites.

In Fig. 4A, B, DMs were classified into 17 sub-classes by class heatmap analysis. "amino acid and its metabolites" enriched the most metabolite numbers (58, 24.17%), followed by "glycerophospholipids" (GP, 37, 15.42%), "fatty acids" (FA, 25, 10.42%), and "heterocyclic compounds" (24, 10.0%). Most proportions of DMs in "amino acid and its metabolites," "GP," and "FA" showed a positive correction with DMs in other sub-classes, while "heterocyclic compounds" contained the most numbers of negative-corrected DMs among sub-classes (Fig. S4). Among obtained DMs, 4-hydroxyhippuric acid showed the highest VIP scores, followed by veliparib, LysoPC 18:0, indoleacetaldehyde, and L-tryptophan (Fig. 5A), while FIGLU showed the highest content with a Log_2FC value of 6.97 among TOP20 VIP DMs (Fig. 5B). Then, eight crucial metabolic genes were selected for expression analysis (Fig. 5C). Relative expressions of *DGAT2*, *PPARγ*, *LIPO*, *CREB3*, *FATP1*, FATP4, and *COQ10* were approximately 62.0-, 6.8-, 83.9-, 5.9-, 11.8-, 4.3-, and 6.6-fold higher in *A. veronii* infection group by comparing with the control, while *NDPK-A* expression decreased sharply ($p < 0.05$).

KEGG analysis revealed that DMs were classified into five subcategories. "Metabolic pathways" contained the most numbers of assigned DMs (63, 75.90%), followed by "biosynthesis of amino acids" (15, 18.07%), "biosynthesis of cofactors" (13, 15.66%), and "2-Oxocarboxylic acid metabolism" (11, 13.25%) (Fig. 6A). In Fig. 6B, annotated DMs in "linoleic acid metabolism" showed the highest tendency towards upregulation among TOP20 KEGG pathways. Then, the relative contents of crucial DMs were further analyzed in four dominant KEGG pathways, including "2-oxocarboxylic acid metabolism," "cysteine and methionine metabolism," "biosynthesis of amino acids," and "aminoacyl-tRNA biosynthesis." KEGG analyses revealed that most numbers of DMs in the above four KEGG pathways belonged to "amino acid and its metabolites" (Fig. S5A-D).

Liver Transcriptome Analysis by RNA-seq

RNA-seq analysis obtained approximately an average of 10.81 G and 10.14 G of clean base from the WCCLCtl group and WCCLAv group with Q_{30} values higher than 94.13% and 94.70%, respectively. A total of 3323 DEGs were obtained in RNA-seq, including 1819 increased DEGs and 1504 decreased DEGs (Fig. S6A-B). Then, the similarities of DEG expression patterns were calculated by K-means clustering analysis (Fig. 7A and Table S1). Seven subclasses of expression patterns were detected in RNA-seq with the highest DEG numbers of 1247 in subclass 1. In Fig. 7B, eight DEGs (*RAD1*, *WAP65-1*, *MBP-C*, *TNFRSF11A*, *p53BP2*, *CFI*, *TRIM39*, and *CFB*) were selected for expression validation of transcriptomic results.

GO analysis revealed that "cellular process" enriched the most DEG numbers (2557, 76.95%) in biological process (BP), possessing 1387 increased DEGs and 1170 decreased DEGs. "Cellular anatomical entity" was the predominant subgroup (2952, 88.84%) in cellular component (CC), containing 1611 increased DEGs and 1341 decreased DEGs. The major subgroup of the transcript was represented by "binding" (2170, 65.30%) in molecular function (MF), possessing 1198 increased DEGs and 972 decreased DEGs (Fig. S7A-B). In addition, "Endoplasmic reticulum (ER) lumen" (88, 19.78%) was the most predominant subclass in TOP50 GO terms, followed by "protein folding" (72, 16.44%) (Fig. S7C).

In Fig. 8A, B, DEGs were classified into six KEGG subcategories. "Metabolic pathway" contained the most numbers of DEGs (455, 10.48%), followed by "protein processing in ER" (107, 18.77%), while the highest proportion of enriched DEGs was observed in "steroid biosynthesis" (26, 49.06%). In Fig. 8C, D, most proportions of DEGs involved in "protein processing in ER" and "steroid biosynthesis" increased dramatically.

Integrated Analysis of Multiomics Results

In Fig. 9A, B, all DEGs and DMs were separated by the O2PLS model. Then, coexpression patterns of DEGs and

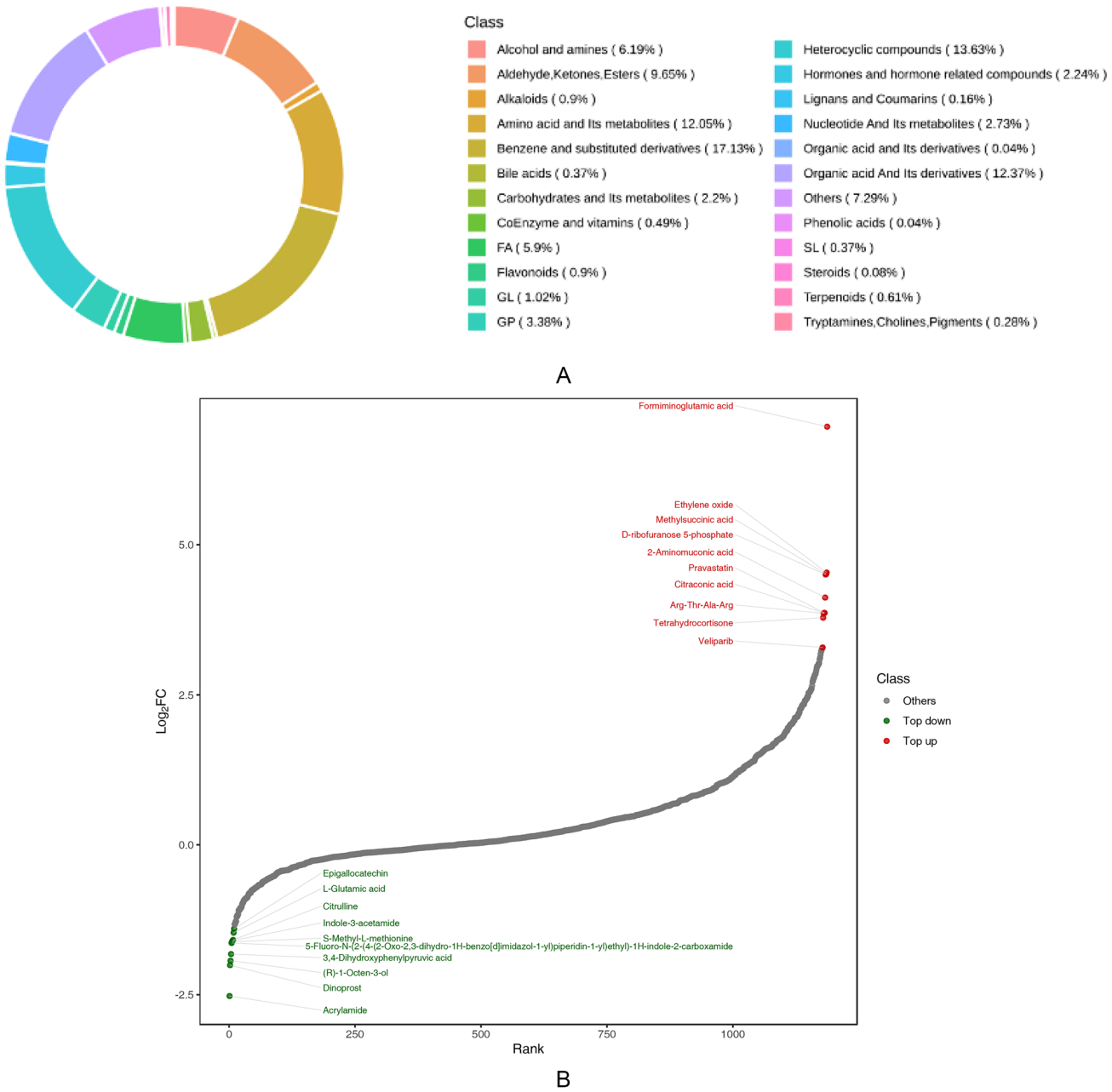

Fig. 3 Metabolic category (**A**) and dynamic distribution (**B**) in the liver of WCC

DMs were analyzed by nine quadrant plots. In Fig. 9C, a positive correlation between DEGs and DMs was shown in the third quadrant (35.68%) and the seventh quadrant (5.39%), while a negative correlation between DEGs and DMs was presented in the first quadrant (54.28%) and the ninth quadrant (4.65%). In Fig. 9D, E, correlation heatmap analysis revealed that positive- or negative-correlated DMs and DEGs may predominantly regulate five subclasses of metabolites, including "amino acid and its metabolites" (24.41%), "GP" (17.76%), "FA" (10.53%), "organic acid and its derivatives" (10.16%), and "heterocyclic compounds" (9.78%).

Integrated analysis of DEGs and DMs revealed that a total of 83 DMs and 1355 DEGs were mapped to 25 shared KEGG pathways (Fig. S8). "Metabolic pathways" enriched the most numbers of DEGs and DMs, followed by "biosynthesis of cofactors" and "biosynthesis of amino acids," while high ratio of DM/DEG was observed in "2-Oxocarboxylic acid metabolism" among pathways (Fig. 10A). In Fig. 10B, "biosynthesis of factors" possessed 18 increased DEGs and 24 decreased DEGs, along with 10 increased DMs and 3 decreased DMs. "Biosynthesis of amino acids" contained 18 increased DEGs and

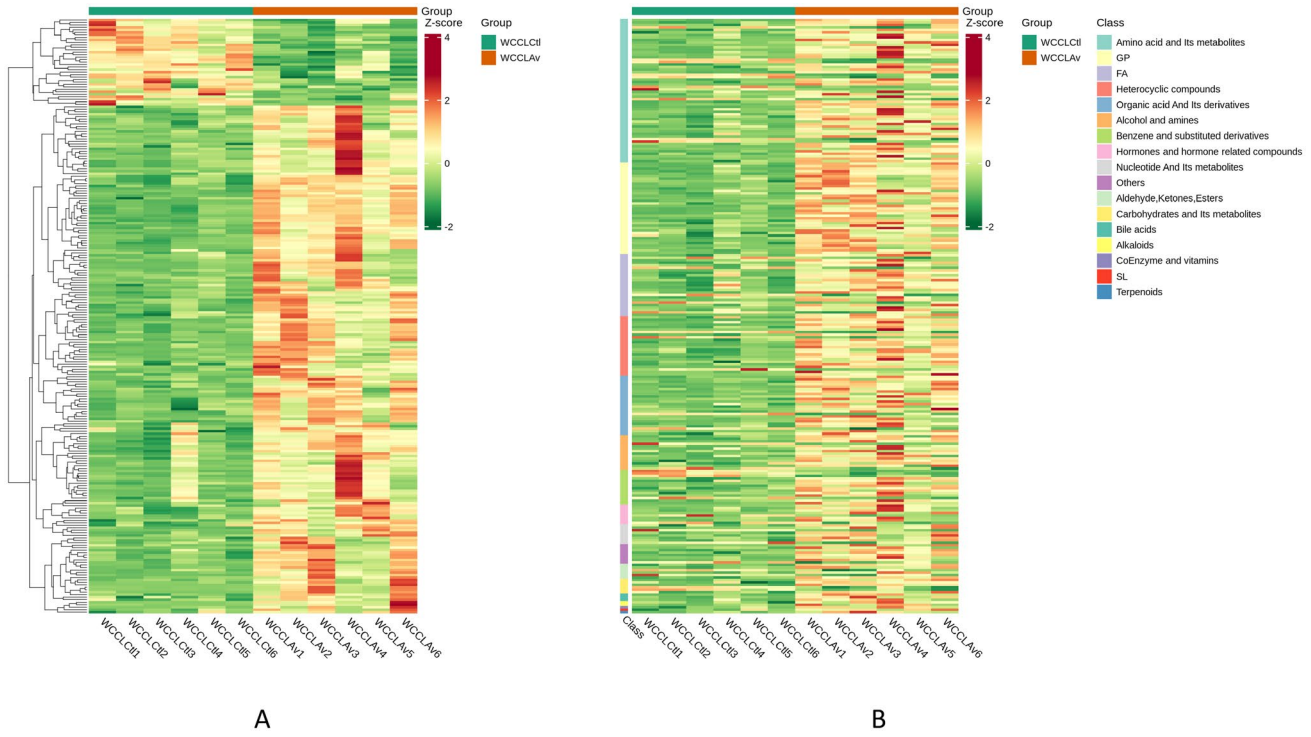

Fig. 4 Feature and classification of DMs. **A** Cluster heatmap analysis of DMs. **B** Class heatmap analysis of DMs

9 decreased DEGs, along with 11 increased DM and 4 decreased DMs. "2-Oxocarboxylic acid metabolism" possessed 6 increased DEGs and 3 decreased DEGs, along with 9 increased DMs and 2 decreased DMs. In addition, L-tryptophan, methionine, L-tyrosine, and L-Glu were the shared DMs that may play important roles in immunometabolic regulation. The correlation network analyses of "biosynthesis of cofactors," "biosynthesis of amino acids," and "2-Oxocarboxylic acid metabolism" are shown in Fig. 10C-H. In this study, amino acids, such as L-Glu, showed the closest correlation with DEGs than other metabolites in "biosynthesis of factors," "biosynthesis of amino acids," and "2-Oxocarboxylic acid metabolism."

To further investigate the comprehensive interplay of all crucial DMs (p-value < 0.05, TOP10 VIP in pathways) and DEGs (p-value < 0.05, $|\log_2 FC| \geq 1$), the pathway network and its detailed information are shown in Fig. 11 and Table S2, respectively. Expression levels of indicator genes were significantly altered in the metabolism of carbohydrates, lipids, amino acids, and nucleotides. In addition, most proportion of DMs increased dramatically in lipid biosynthesis and conversion processes of metabolic intermediates of organic acids, nucleotides, and amino acids, whereas metabolic processes of carbohydrates appeared to be inactivated in the liver of WCC after the *A. veronii* challenge.

Discussion

A. veronii Infection Elevates Immune Response in Tissues of WCC

A. veronii is a gram-negative pathogenic bacteria that can trigger severe disease outbreak in aquaculture and pose a great threat to the health of farmed fish (Li et al. 2020). In addition, *A. veronii* is broadly distributed in freshwater environments, which plays a dominant role in motile aeromonad septicemia (MAS) of cyprinid fish in southern China (Ran et al. 2018). The current study revealed that expression levels of the *aerA* gene upregulated sharply in the liver, kidney, spleen, and intestine of WCC following *A. veronii* challenge, along with the significantly altered levels of disease-related enzymatic activities and immune gene expressions. Previous studies have demonstrated that AKP, AST, ACP, and ALT were the crucial disease-related enzymes associated with organ damage in fish after the exposure to stressors (Ma et al. 2018). Among the immune properties, fish *MHC-I* can directly initiate an immune response to invading pathogens (Grimholt 2016), while *HSP70* plays an important role in response to environmental stressors (Yamashita et al. 2010). *CD3* can mediate T cell activation and phagocyte-regulated immunity by interaction with *CD4* (Portoles et al. 1950). *IGF* can increase

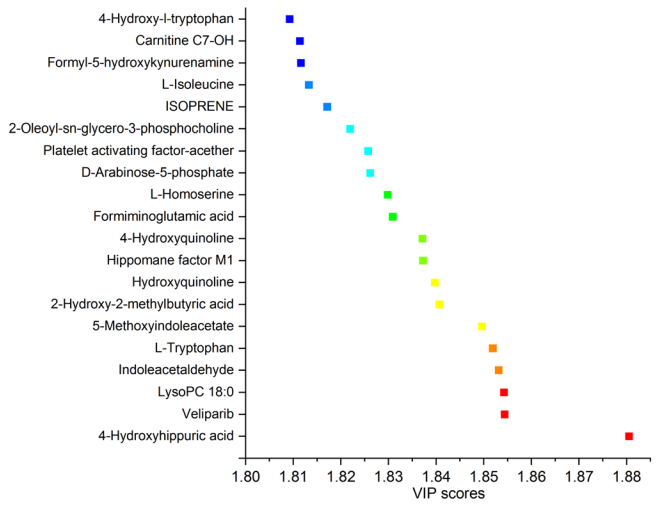

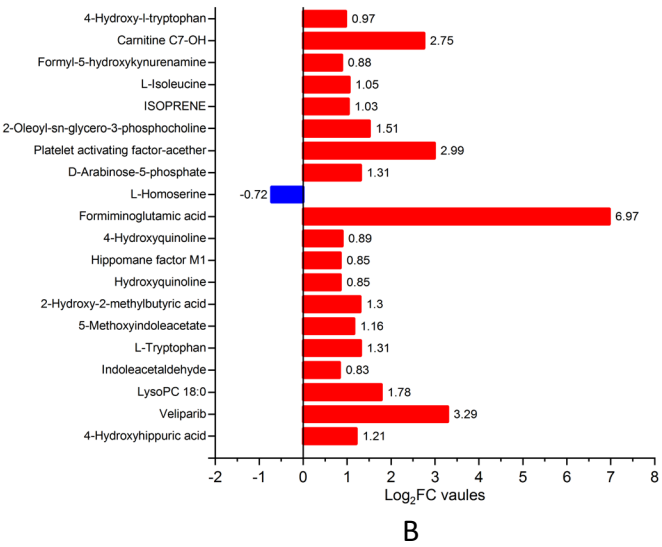

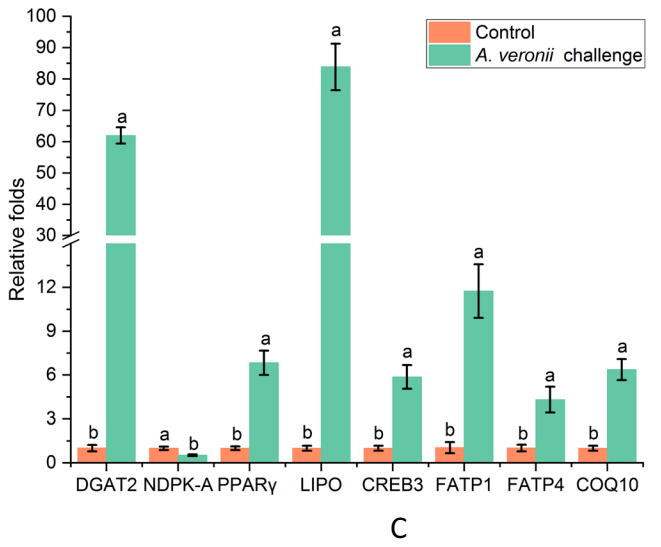

Fig. 5 Determination of crucial DMs and metabolic gene expressions. **A** Identification of crucial DMs by VIP scores. **B** Log_2FC values of crucial T20 VIP DMs. **C** Metabolic gene expressions in the liver of WCC following *A. veronii* challenge. Relative gene expressions were calculated by the $2^{-\Delta\Delta Ct}$ methods. The calculated data (mean ± SD) with different letters were significantly different ($p < 0.05$)

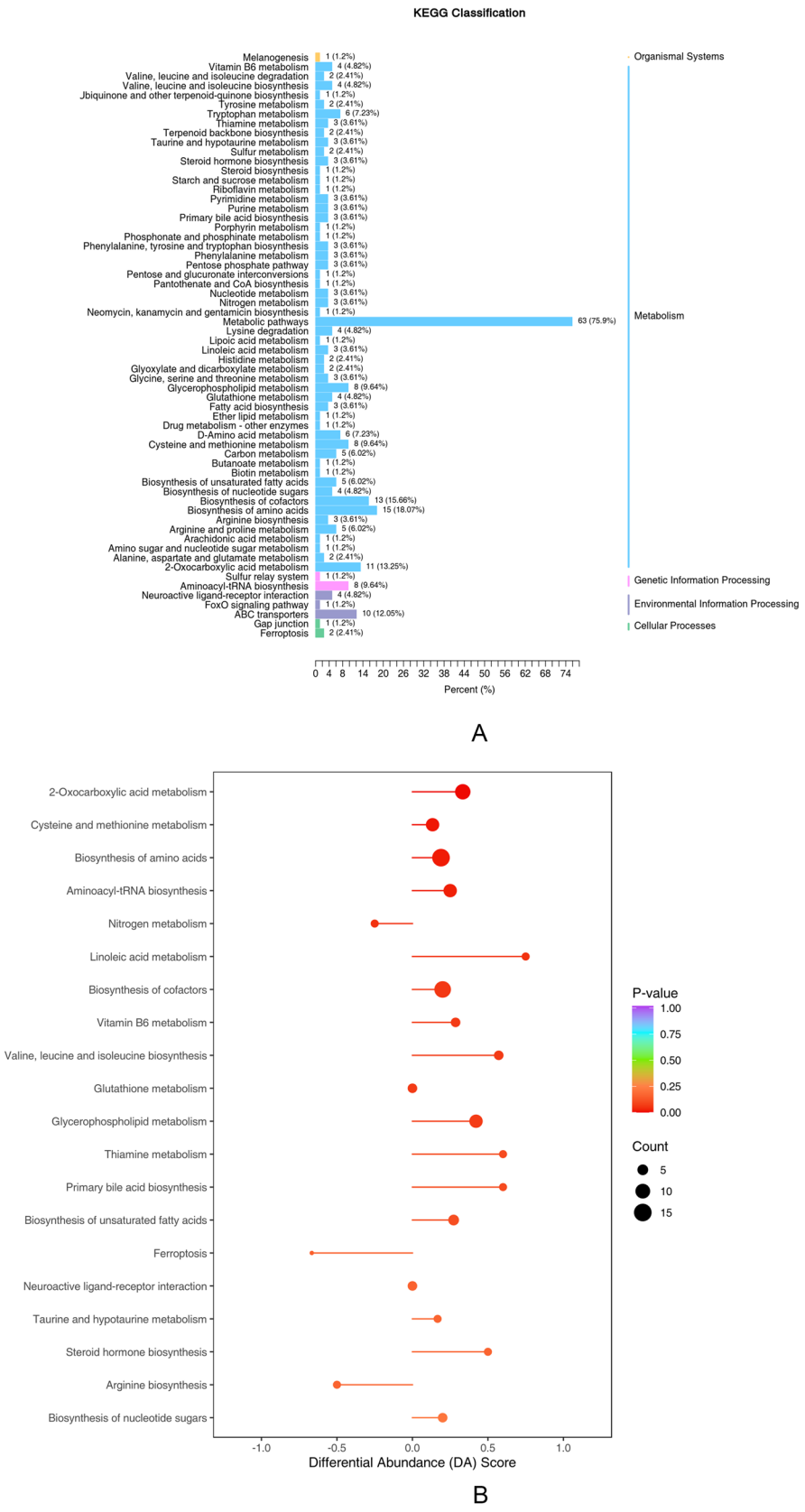

Fig. 6 Metabolic signal pathways in the liver of WCC following *A. veronii* challenge. **A** KEGG classification of annotated DMs. **B** KEGG pathway of annotated DMs with the calculation of DA score

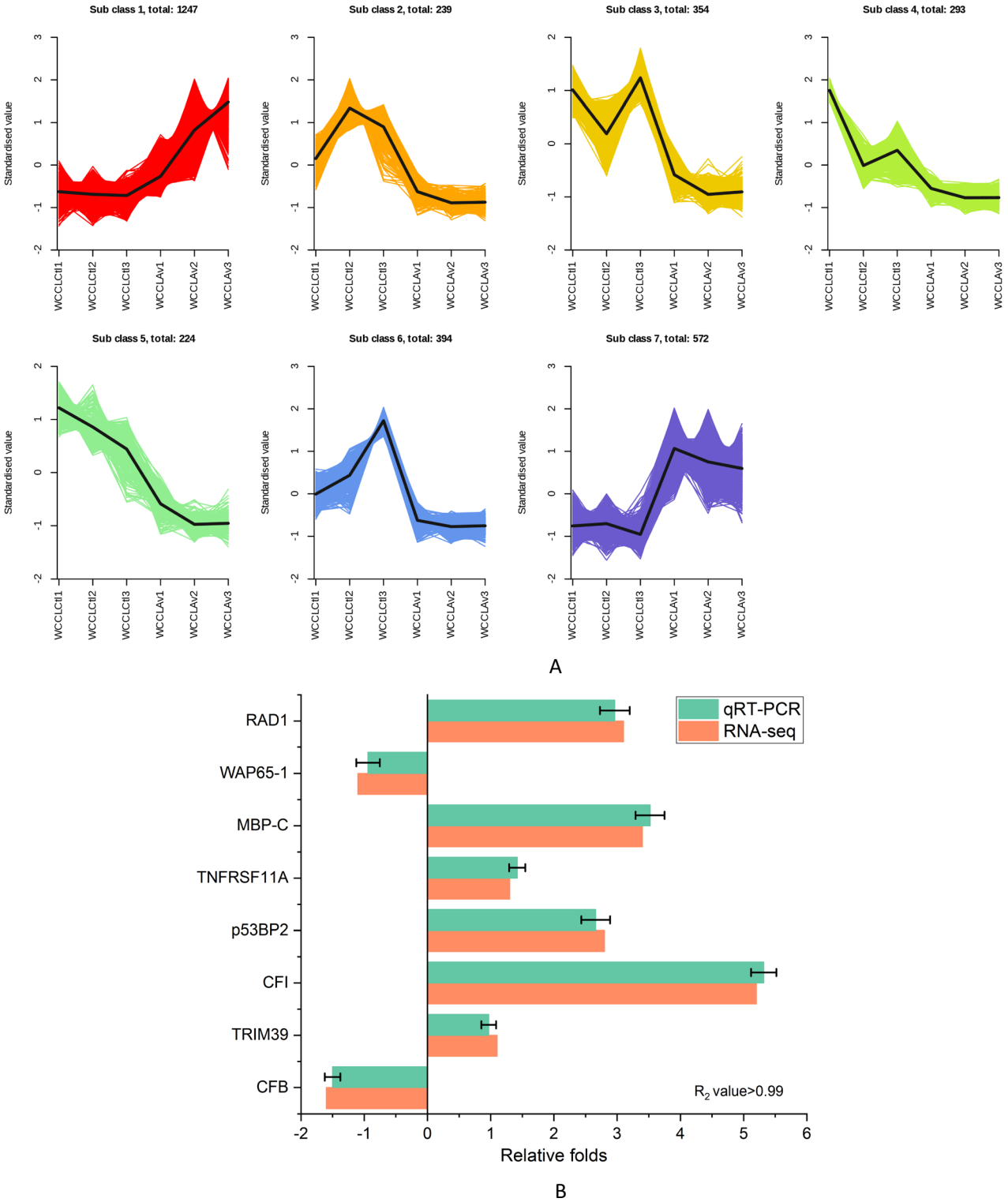

Fig. 7 Characterization of RNA-seq data. **A** Expression patterns of DEGs calculated by K-means clustering analysis. **B** Validation of RNA-seq data by qRT-PCR assay

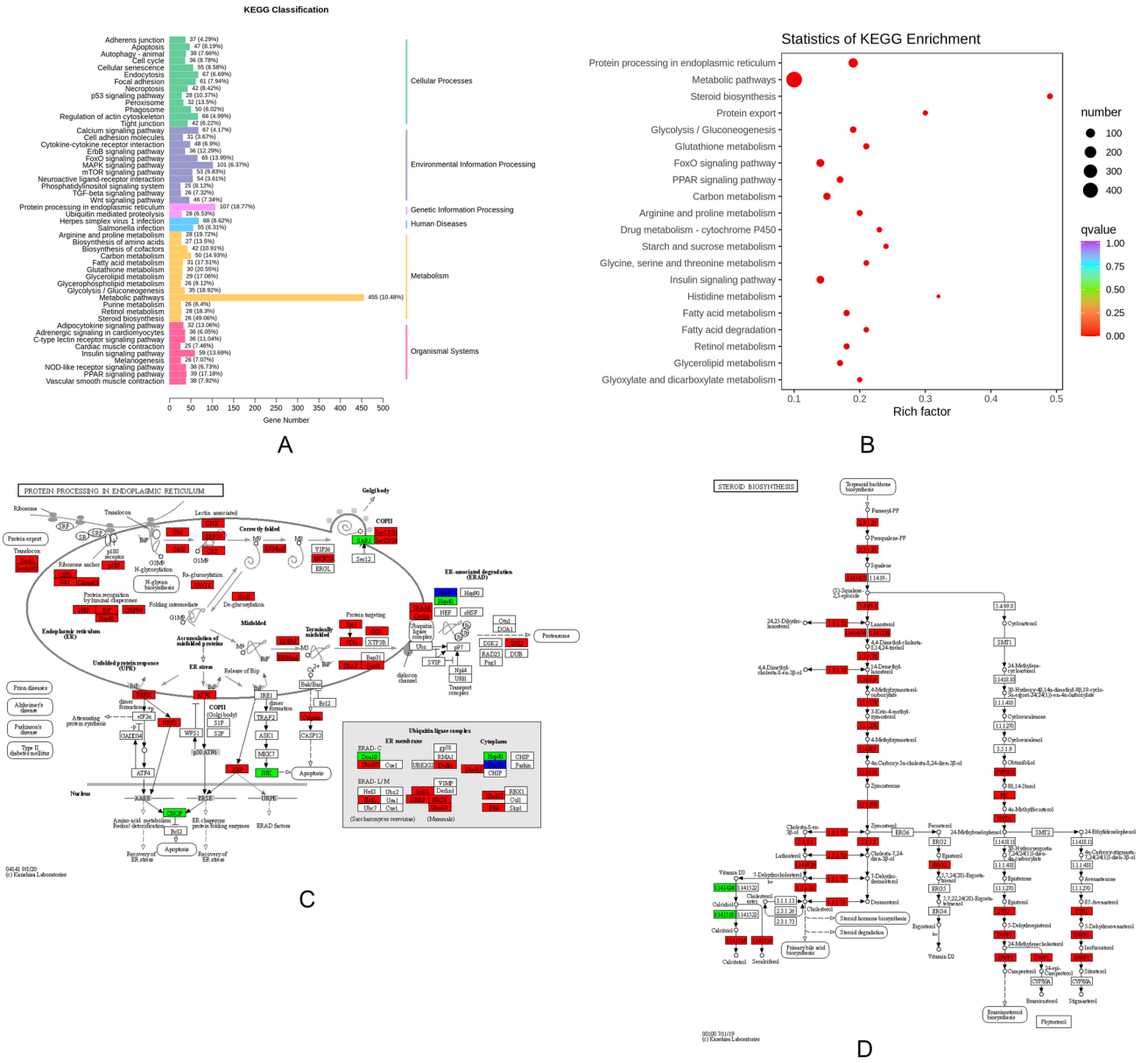

Fig. 8 DEG statistics by KEGG analysis. **A** Gene proportion calculated by KEGG classification. **B** DEGs analyzed by Top 20 KEGG enrichment. Sizes of circles represented the numbers of enriched DEGs. A Significant difference was distinguished from blue to red. **C**, **D** Crucial DEGs were determined in the protein process in ER and steroid biosynthesis. Increased, decreased and no significant changed expressions of DEGs were marked in red, green, and blue, respectively

the immune activity of leukocytes and phagocytes in fish (Franz et al. 2016). *ApoD* is recently identified as one of the important antimicrobial genes from the transcriptome of *A. hydrophila*–infected fish (Gao et al. 2024). *LysC* is one of the crucial antimicrobial peptide (AMP) genes involved in immune defense against bacterial infection (Plotka et al. 2020). These results suggested that *A. veronii* infection could dramatically regulate immune response in WCC. However, the global understanding of pathological response in *A. veronii*–infected WCC remains unclear.

Antioxidant Collapse and Metabolic Signals in the Liver

Stressor exposure may alter physiological response, including hormone level, metabolite abundance, and hydromineral modulation, to balance homeostasis and reduce stress-induced adverse efforts in fish (Barton 2002). As is well known, the liver is one of the pivotal organs that can participate in immune regulation, detoxication, and nutritional metabolism (Bruslé and i Anadon GG. 2017). Although

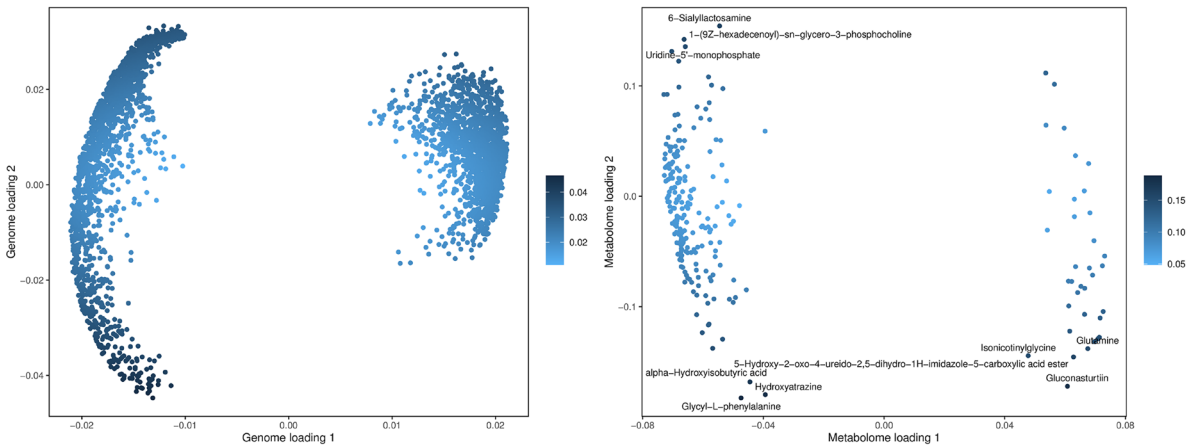
Genome loading 2
Genome loading 1
0.02
0.00
−0.02
−0.04
−0.02
−0.01
0.00
0.01
0.02
0.04
0.03
0.02
Metabolome loading 2
Metabolome loading 1
0.1
0.0
−0.1
−0.08
−0.04
0.00
0.04
0.08
0.15
0.10
0.05
6−Sialyllactosamine
1−(9Z−hexadecenoyl)−sn−glycero−3−phosphocholine
Uridine−5'−monophosphate
Isonicotinylglycine
Glutamine
5−Hydroxy−2−oxo−4−ureido−2,5−dihydro−1H−imidazole−5−carboxylic acid ester
alpha−Hydroxyisobutyric acid
Gluconasturtiin
Hydroxyatrazine
Glycyl−L−phenylalanine

A B

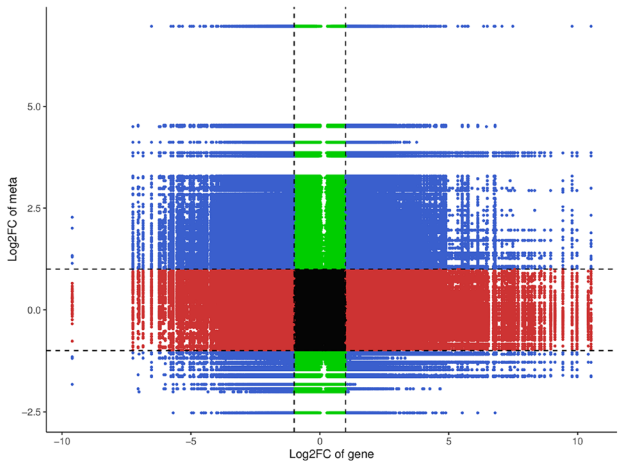
Log2FC of meta
Log2FC of gene
5.0
2.5
0.0
−2.5
−10
−5
0
5
10

C

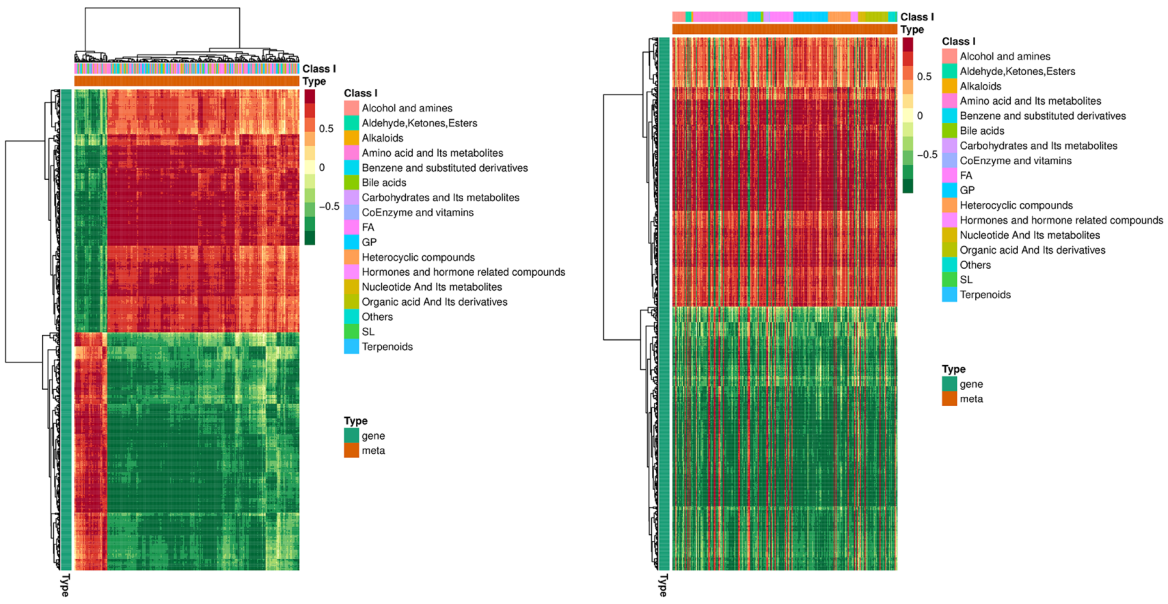
Class I
Type
0.5
0
−0.5
Class I
Alcohol and amines
Aldehyde,Ketones,Esters
Alkaloids
Amino acid and Its metabolites
Benzene and substituted derivatives
Bile acids
Carbohydrates and Its metabolites
CoEnzyme and vitamins
FA
GP
Heterocyclic compounds
Hormones and hormone related compounds
Nucleotide And Its metabolites
Organic acid And Its derivatives
Others
SL
Terpenoids
Type
gene
meta
Type

D E

◂**Fig. 9** Integrated analysis of RNA-seq and LC–MS/MS. **A**, **B** DEGs and DMs were analyzed by O2PLS models. **C** Co-expression patterns of DEGs and DMs were analyzed by nine quadrant plots. Genes and metabolites without differential expression were presented in the fifth quadrant. Co-expression patterns of DEGs and DMs showing positive correlation were presented in the third and seventh quadrants. Co-expression patterns of DEGs and DMs showing negative correlation were presented in the first and ninth quadrants. Co-expression patterns of DEGs and DMs possessing no correlations were presented in the second, fourth, sixth, and eighth quadrants. **D**, **E** Correlation heatmap analysis of DEGs and DMs

antioxidant enzymes and endogenous antioxidants can directly diminish cytokine-stimulated cytotoxicity (Lortz et al. 2000), severe oxidative damage may impair redox balance and mitochondrial dysfunction (Lushchak 2011). Furthermore, excessive ROS accumulation may strongly impair host antioxidant immunity, attenuate metabolic response, and reduce the elimination mechanism of invading bacteria (Su et al. 2018). In this study, *A. veronii* infection could stimulate various ranges of tissue damage in the liver of WCC. Moreover, the enzymatic activity of CAT, GPx, GR, MAO, and SDH in the liver decreased sharply after the *A. veronii* challenge, while LDH activity markedly increased. Invasive bacteria can promote redox imbalance and mitochondrial dysfunction in host tissues undergoing oxidative injury, which may be associated with metabolic disorder and immune abnormality (Engelmann et al. 2021). In this study, DEGs of protein processing in ER and steroid biosynthesis were markedly altered after *A. veronii* infection. In general, ER, an important organelle for the biosynthesis of proteins, carbohydrates, and lipids, can transport soluble immune effectors and contribute to host defense against invading pathogens via autophagy, but some invading pathogens may disrupt ER function to avoid the immune surveillance process within the host (Roy et al. 2006). This result suggested that *A. veronii* infection may cause antioxidant collapse, alter the metabolic process, and facilitate liver injury of WCC.

Determination of Immunometabolic Interplay in the Liver

To discover the immunometabolic interplay in WCC after the *A. veronii* challenge, multiomics analyses were performed. In this investigation, a total of 83 DMs and 1355 DEGs were mapped to 25 shared KEGG pathways. Most proportions of DEGs and DMs increased significantly in the metabolic conversion of lipids, amino acids, nucleotides, and organic acids, while high proportions of DMs belonging to amino acids, lipids, and heterocyclic intermediates showed a positive correlation with other DMs. Most portions of DEGs in metabolic processes, including *DGAT2*, *PPARγ*, *LIPO*, *CREB3*, *FATP1*, *FATP4*, and *COQ10*, increased markedly in WCC after *A. veronii* infection. In general, carbon and lipid metabolism not only provide energy for cell development, but also participate in immune regulation and physiological response (Head et al. 2014; Choi et al. 2021). Metabolic products of the tricarboxylic acid (TCA) cycle can be involved in macrophage activation and cytokine secretion (Zhao et al. 2020a), while localization of fatty acids into distinct cellular pools may display a direct impact on immune function, including antigen presentation and immune cell response (Yaqoob and Calder 2007). Among known fatty acids and conjugates, mevalonic acid is a unique intermediate that can determine the synthesis of steroids and steroid derivates (Bryson and Sweat 1962). Recent findings indicate that steroid hormones can alleviate pathophysiological levels (Ben-Nathan et al. 1999) and generate antimicrobial peptides (Marin-Luevano et al. 2021). Amino acids are found to be preferential energy substrates together with lipids (Jia et al. 2021), but their deficiency may impair immune function and attenuate host resistance against infectious diseases (Li et al. 2007). Besides, biosynthesis of cofactors, biosynthesis of amino acids, and 2-oxocarboxylic acid metabolism appeared to be crucial points of immunometabolic mechanism in response to *A. veronii* infection. Most increased DMs belonged to aromatic amino acids (AAAs) and branch-chain amino acids (BCAAs). In general, BCAAs not only provide acetyl-CoA derivatives that can be involved in mTOR-mediated immune activation (Kelly and Pearce 2020), but also support lymphocyte proliferation to reduce susceptibility to invading pathogens (Calder 2006). AAAs and their derivatives can act as crucial signals in the interplay between host and microbes, which can confer host protection against invading pathogens and ameliorate pathogen-induced inflammatory response (Anand et al. 2024). In addition, amino acids, such as L-Glu, showed the closest correlation with DEGs in the above three pathways. FIGLU showed the highest content among TOP20 VIP DMs, whereas 4-hydroxyhippuric acid should be identified as one of the crucial liver biomarkers with the highest VIP score. FIGLU generated in the liver by a histidase reaction can be rapidly converted to Glu, but its accumulation may reflect the impairment of folate metabolism in the liver, which may dramatically reduce Glu conversion and glutamine (Gln) supply (Holeček 2020). L-Glu, one of dispensable amino acids in fish, can serve as important regulator involved in nutrient utilization, biosynthesis of glutathione (GSH) for antioxidant function, and immune defense against invading pathogens through activation of immune cells (Zhao et al. 2020b; Newsholme et al. 2003; Jiang et al. 2016). Phenolic acid, including 4-hydroxyhippuric acid, is the metabolic product of tyrosine that can be considered crucial parameter of metabolic ability in the liver (Liebich and Pickert 1985). Moreover, hydroxyhippuric acid can enhance the immune function and migration ability of immune cells via aryl hydrocarbon receptor (AhR) signals (Tang et al. 2023).

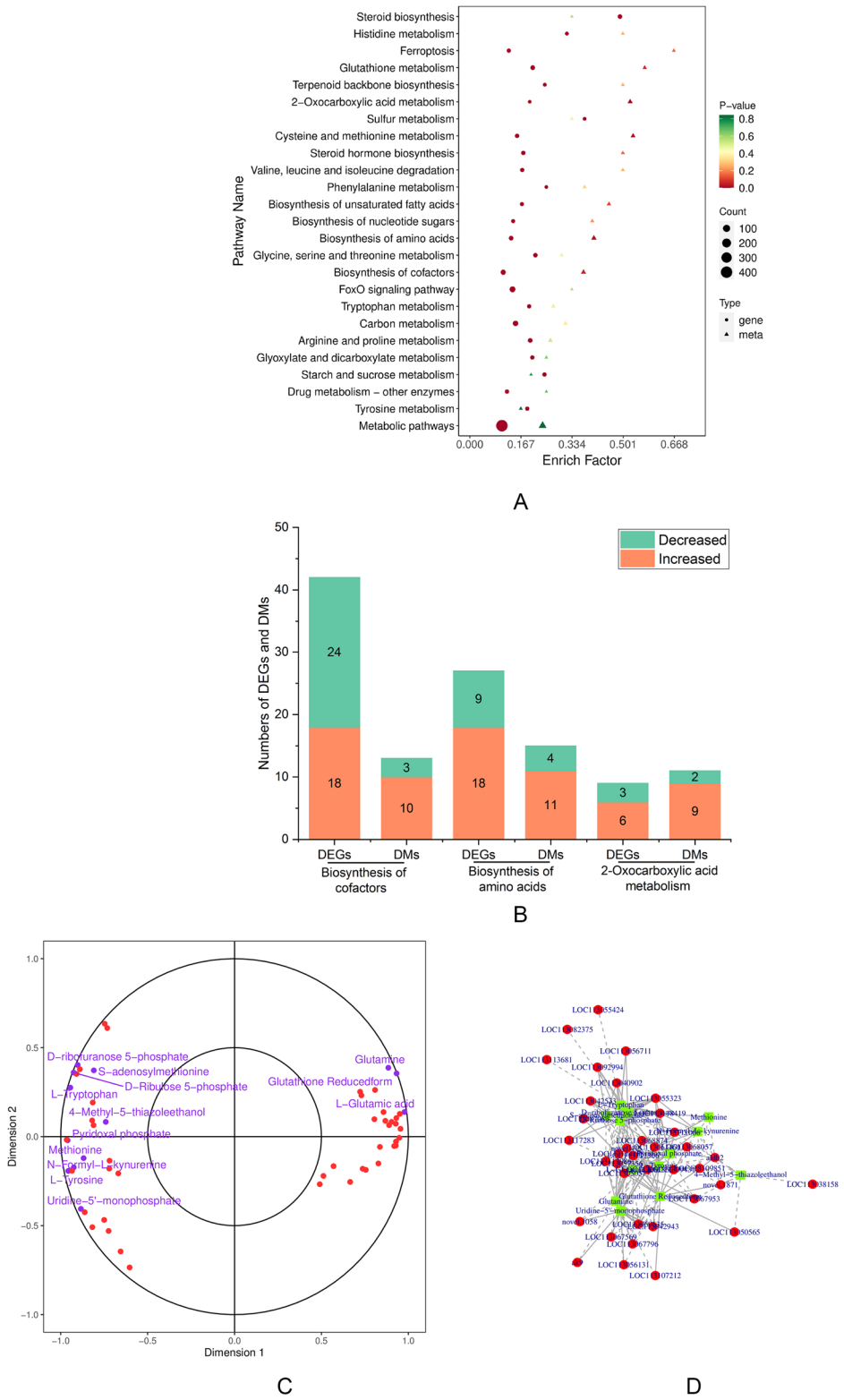

Fig. 10 Shared KEGG pathways of DEGs and DMs. **A** Co-enrichment of DEGs and DMs in shared KEGG pathways. Sizes of circles and triangles represented the enriched numbers of DEGs and DMs, respectively. A significant difference was distinguished from green to red. **B** Numbers of DEGs and DMs in "Biosynthesis of cofactors," "Biosynthesis of amino acids," and "2-Oxocarboxylic acid metabolism." **C**, **D** The correlation of DEGs and DMs in "Biosynthesis of cofactors." **E**, **F** The correlation of DEGs and DMs in "Biosynthesis of amino acids." **G**, **H** The correlation of DEGs and DMs in "2-Oxocarboxylic acid metabolism."

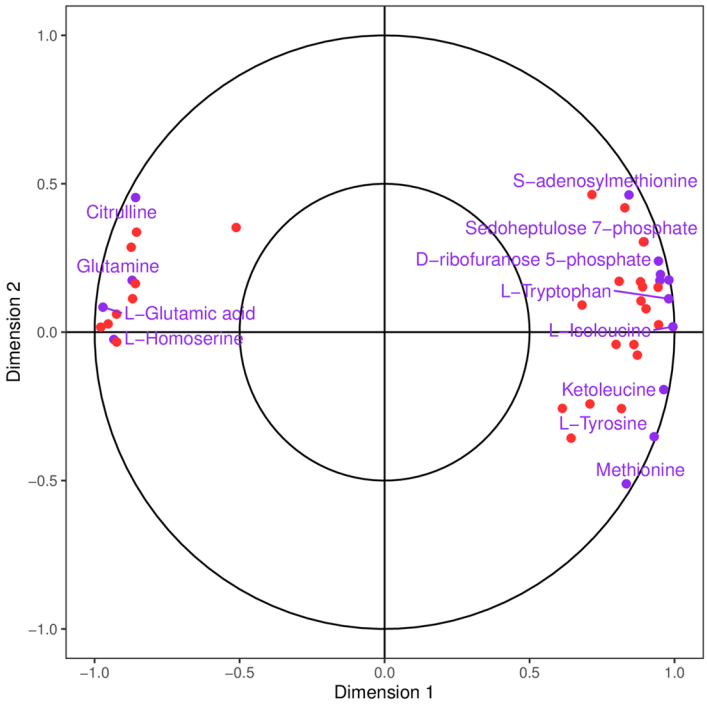

E

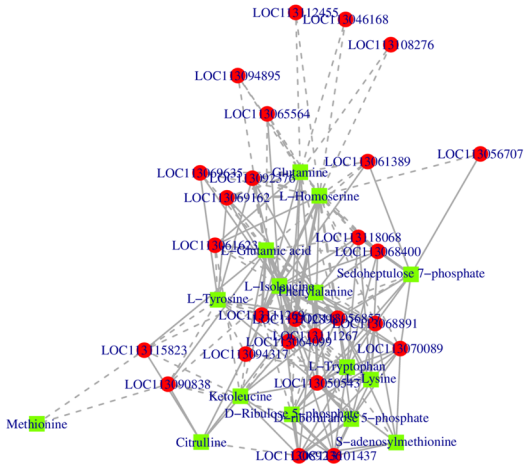

F

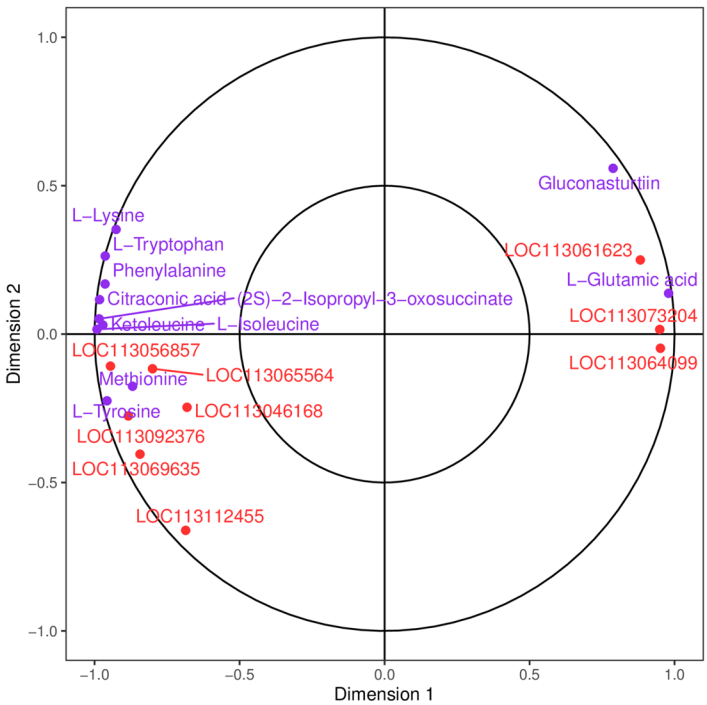

G

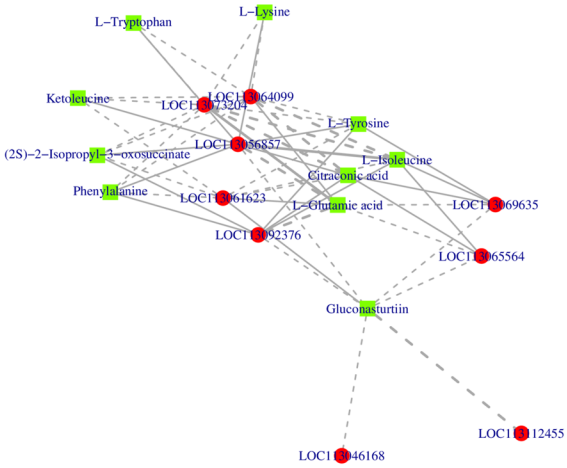

H

Fig. 10 (continued)

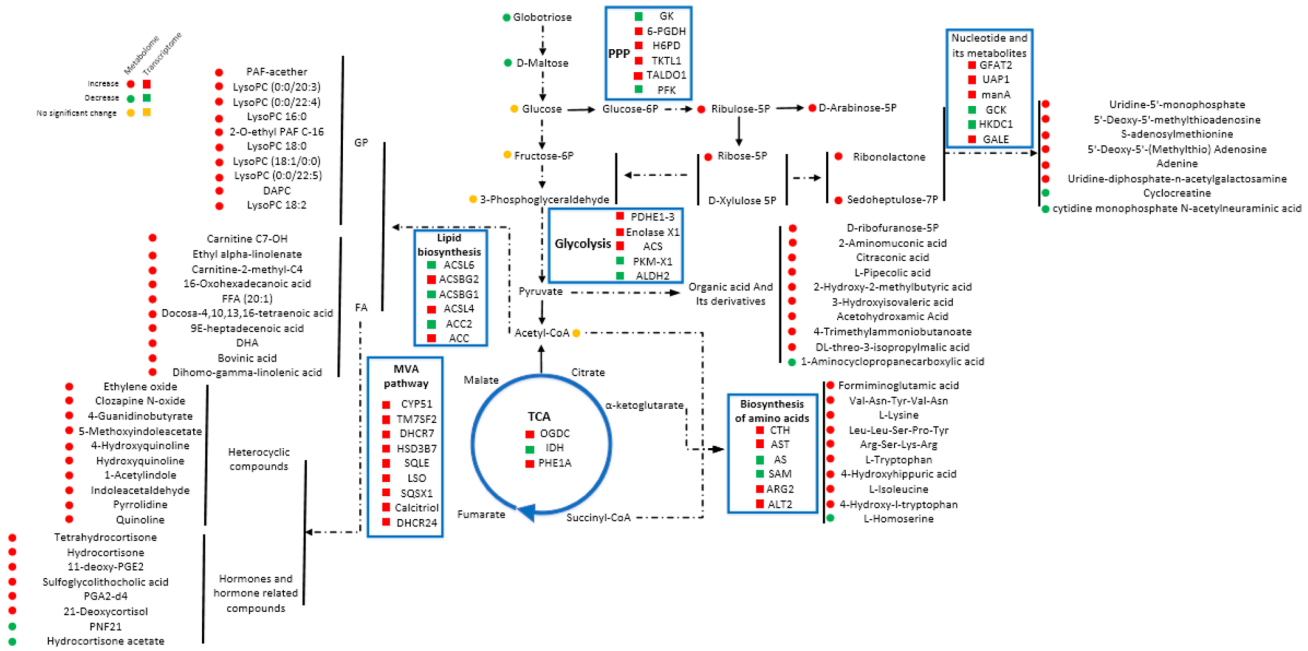

Fig. 11 Interactive network analysis of DEGs and DMs in the liver of WCC following *A. veronii* challenge. DEGs and DMs were indicated by squares and circles, respectively

Thus, taken together, *A. veronii* infection promoted oxidative stress-induced tissue injury and displayed a profound impact on metabolic processes of lipids, amino acids and carbohydrates in WCC via ER dysfunction.

Conclusion

In summary, we characterized pathological detection, antioxidant status metabolic features, and identification of hub genes involved in immunometabolism of WCC after the *A. veronii* challenge. In addition, metabolic products of amino acids, such as FIGLU, L-Glu, and 4-hydroxyhippuric acid, were considered the crucial liver biomarkers in *A. veronii*–infected WCC. This study indicated that *A. veronii* infection may predominantly dysregulate ER function to affect metabolic processes, especially the amino acid metabolism.

Supplementary Information The online version contains supplementary material available at https://doi.org/10.1007/s10126-024-10347-3.

Author contributions Fei Wang performed the methodology, data curation, and formal analysis; Zi-Rou Zhong, Qing Xie, and Jie Ou performed the formal analysis and validation; Ning-Xia Xiong and Ming-Zhu Huang performed the formal analysis; Shi-Yun Li, Gang Hu, and Zi-Le Qin performed the validation; Sheng-Wei Luo performed the conceptualization, supervision, project management, and article writing.

Funding This research was supported by the National Key Research and Development Program of China, China (grant no. 2023YFD2401601), the National Natural Science Foundation of China, China (grant no. 31902363), and the Hunan Provincial Natural Science Foundation of China, China (grant no. 2021JJ40340).

Data Availability No datasets were generated or analyzed during the current study.

Declarations

Ethical Approval All applicable international, national, and/or institutional guidelines for the care and use of animals were followed. All experimental procedures were conducted following Chinese animal welfare laws, guidelines, and policies (GB/T 35892–2018).

Conflict of Interests The authors declare that they have no conflict of interest.

References

Anand G, Clark-Dinovo C, Perry AM, Goodwin VM, St Raymond E, Sakleshpur S et al (2024) Aromatic amino acid metabolites alter interferon signaling and influenza pathogenesis. Front Mol Biosci 10:1232573

Barton BA (2002) Stress in fishes: a diversity of responses with particular reference to changes in circulating corticosteroids. Integr Comp Biol 42:517–525

Ben-Nathan D, Padgett DA, Loria RM (1999) Androstenediol and dehydroepiandrosterone protect mice against lethal bacterial infections and lipopolysaccharide toxicity. J Med Microbiol 48:425–431

Bernard Q, Smith AA, Yang X, Koci J, Foor SD, Cramer SD et al (2018) Plasticity in early immune evasion strategies of a bacterial pathogen. Proc Natl Acad Sci 115:E3788–E3797

Bols NC, Brubacher JL, Ganassin RC, Lee LE (2001) Ecotoxicology and innate immunity in fish. Dev Comp Immunol 25:853–873
Bruslé J, i Anadon GG (2017) The structure and function of fish liver. Fish morphology. Routledge, pp 77–93
Bryson MJ, Sweat ML (1962) Is mevalonic acid a precursor of the corticosteroids? Arch Biochem Biophys 96:1–3
Calder PC (2006) Branched-chain amino acids and immunity. J Nutr 136:288S-293S
Chen C, Wang J, Pan D, Wang X, Xu Y, Yan J et al (2023) Applications of multi-omics analysis in human diseases. MedComm 4:e315
Choi I, Son H, Baek J-H (2021) Tricarboxylic acid (TCA) cycle intermediates: regulators of immune responses. Life 11:69
Engelmann C, Clària J, Szabo G, Bosch J, Bernardi M (2021) Pathophysiology of decompensated cirrhosis: portal hypertension, circulatory dysfunction, inflammation, metabolism and mitochondrial dysfunction. J Hepatol 75:S49–S66
Franz A-C, Faass O, Köllner B, Shved N, Link K, Casanova A et al (2016) Endocrine and local IGF-I in the bony fish immune system. Biology 5:9
Gao J-h, Zhao J-l, Yao X-l, Tola T, Zheng J, Xue W-b et al (2024) Identification of antimicrobial peptide genes from transcriptomes in Mandarin fish (Siniperca chuatsi) and their response to infection with Aeromonas hydrophila. Fish Shellfish Immunol 144:109247
Grimholt U (2016) MHC and evolution in teleosts. Biology 5:6
Head BP, Patel HH, Insel PA (2014) Interaction of membrane/lipid rafts with the cytoskeleton: impact on signaling and function: membrane/lipid rafts, mediators of cytoskeletal arrangement and cell signaling. Biochim Biophys Acta Biomembranes 1838: 532–545
Holeček M (2020) Histidine in health and disease: metabolism, physiological importance, and use as a supplement. Nutrients 12:848
Ibrahim RE, Elshobaky G, ElHady M, Abdelwarith AA, Younis EM, Rhouma NR et al (2024) Nelumbo nucifera synthesized selenium nanoparticles modulate the immune-antioxidants, biochemical indices, and pro/anti-inflammatory cytokines pathways in Oreochromis niloticus infected with Aeromonas veronii. Fish Shellfish Immunol 144:109287
Jia S, Li X, He W, Wu G (2021) Oxidation of energy substrates in tissues of fish: Metabolic significance and implications for gene expression and carcinogenesis. Amino acids in nutrition and health. Springer, pp 67–83
Jiang J, Wu X-Y, Zhou X-Q, Feng L, Liu Y, Jiang W-D et al (2016) Glutamate ameliorates copper-induced oxidative injury by regulating antioxidant defences in fish intestine. Br J Nutr 116:70–79
Kelly B, Pearce EL (2020) Amino assets: how amino acids support immunity. Cell Metab 32:154–175
Lercher A, Baazim H, Bergthaler A (2020) Systemic immunometabolism: challenges and opportunities. Immunity 53:496–509
Li P, Yin Y-L, Li D, Kim SW, Wu G (2007) Amino acids and immune function. Br J Nutr 98:237–252
Li T, Raza SHA, Yang B, Sun Y, Wang G, Sun W et al (2020) Aeromonas veronii infection in commercial freshwater fish: a potential threat to public health. Animals 10:608
Li S-Y, Xiong N-X, Li K-X, Huang J-F, Ou J, Wang F et al (2024) Cloning, expression and functional characterization of recombinant tumor necrosis factor α1 (TNFα1) from white crucian carp in gut immune regulation. Int J Biol Macromol 254:127770
Li Z, Wang ZW, Wang Y, Gui JF (2018) Crucian carp and gibel carp culture. Aquaculture in China: success stories and modern trends. Wiley, pp 149–157
Liebich HM, Pickert A (1985) Gas chromatographic profiling of phenolic acids in urine of patients with chirrhosis of the liver. J Chromatogr B Biomed Sci Appl 338:25–32
Lortz S, Tiedge M, Nachtwey T, Karlsen AE, Nerup J, Lenzen S (2000) Protection of insulin-producing RINm5F cells against cytokine-mediated toxicity through overexpression of antioxidant enzymes. Diabetes 49:1123–1130
Lu X, Zhao X, Bai C, Zhao C, Lu G, Xu G (2008) LC–MS-based metabonomics analysis. J Chromatogr B 866:64–76
Lushchak VI (2011) Environmentally induced oxidative stress in aquatic animals. Aquat Toxicol 101:13–30
Ma J, Li X, Cui M, Li W, Li X (2018) Negative impact of the imidazolium-based ionic liquid [C8mim] Br on silver carp (Hypophthalmichthys molitrix): long-term and low-level exposure. Chemosphere 213:358–367
Maekawa S, Wang P-C, Chen S-C (2019) Comparative study of immune reaction against bacterial infection from transcriptome analysis. Front Immunol 10:153
Magnadottir B (2010) Immunological control of fish diseases. Mar Biotechnol 12:361–379
Marin-Luevano SP, Rodriguez-Carlos A, Jacobo-Delgado Y, Valdez-Miramontes C, Enciso-Moreno JA, Rivas-Santiago B (2021) Steroid hormone modulates the production of cathelicidin and human β-defensins in lung epithelial cells and macrophages promoting Mycobacterium tuberculosis killing. Tuberculosis 128:102080
Newsholme P, Procopio J, Lima MMR, Pithon-Curi TC, Curi R (2003) Glutamine and glutamate—their central role in cell metabolism and function. Cell Biochem Funct 21:1–9
Plotka M, Szadkowska M, Håkansson M, Kovačič R, Al-Karadaghi S, Walse B et al (2020) Molecular characterization of a novel lytic enzyme LysC from Clostridium intestinale URNW and its antibacterial activity mediated by positively charged N-terminal extension. Int J Mol Sci 21:4894
Portoles P, Rojo J, Golby A, Bonneville M, Gromkowski S, Greenbaum L et al (1989) Monoclonal antibodies to murine CD3 epsilon define distinct epitopes, one of which may interact with CD4 during T cell activation. J Immunol (Baltimore, Md.: 1950) 142:4169–4175
Qi Z-H, Liu Y-F, Wang W-N, Wu X, Xin Y, Lu Y-F et al (2011) Molecular characterization and functional analysis of a complement C3 molecule in the orange-spotted grouper (Epinephelus coioides). Fish Shellfish Immunol 31:1284–1290
Ran C, Qin C, Xie M, Zhang J, Li J, Xie Y et al (2018) Aeromonas veronii and aerolysin are important for the pathogenesis of motile aeromonad septicemia in cyprinid fish. Environ Microbiol 20:3442–3456
Roy CR, Salcedo SP, Gorvel J-PE (2006) Pathogen–endoplasmic-reticulum interactions: in through the out door. Nat Rev Immunol 6:136–147
Secombes C, Wang T, Hong S, Peddie S, Crampe M, Laing K et al (2001) Cytokines and innate immunity of fish. Dev Comp Immunol 25:713–723
Stoliar OB, Lushchak VI (2012) Environmental pollution and oxidative stress in fish. Oxidative stress-environmental induction and dietary antioxidants. InTech, pp 131–166
Su Y-C, Jalalvand F, Thegerström J, Riesbeck K (2018) The interplay between immune response and bacterial infection in COPD: focus upon non-typeable haemophilus influenzae. Front Immunol 9:2530
Tang JS, Stephens R, Li Y, Cait A, Gell K, Faulkner S et al (2023) Polyphenol and glucosinolate-derived AhR modulators regulate GPR15 expression on human CD4+ T cells. J Nutr Biochem 122:109456
Wang L, Fan C, Xu W, Zhang Y, Dong Z, Xiang J et al (2017) Characterization and functional analysis of a novel C1q-domain-containing protein in Japanese flounder (Paralichthys olivaceus). Dev Comp Immunol 67:322–332
Wu N, Song Y-L, Wang B, Zhang X-Y, Zhang X-J, Wang Y-L et al (2016) Fish gut-liver immunity during homeostasis or inflammation revealed by integrative transcriptome and proteome studies. Sci Rep 6:1–17

Xiong N-X, Mao Z-W, Ou J, Fan L-F, Chen Y, Luo S-W et al (2022) Metabolite features and oxidative response in kidney of red crucian carp (Carassius auratus red var) after Aeromonas hydrophila challenge. Comp Biochem Physiol c: Toxicol Pharmacol 255:109293

Xiong N-X, Wang F, Luo W-S, Ou J, Qin Z-L, Huang M-Z et al (2023) Tumor necrosis factor α2 (TNFα2) facilitates gut barrier breach by *Aeromonas hydrophila* and exacerbates liver injury in hybrid fish. Aquaculture 577:739995

Yamashita M, Yabu T, Ojima N (2010) Stress protein HSP70 in fish. Aqua BioSci Monogr 3:111–141

Yang J, Wang D, Li Y, Wang H, Hu Q, Wang Y (2023) Metabolomics in viral hepatitis: advances and review. Front Cell Infect Microbiol 13:1189417

Yaqoob P, Calder PC (2007) Fatty acids and immune function: new insights into mechanisms. Br J Nutr 98:S41–S45

Zhao H, Raines LN, Huang SC-C (2020a) Carbohydrate and amino acid metabolism as hallmarks for innate immune cell activation and function. Cells 9:562

Zhao Y, Zhang T-R, Li Q, Feng L, Liu Y, Jiang W-D et al (2020b) Effect of dietary L-glutamate levels on growth, digestive and absorptive capability, and intestinal physical barrier function in Jian carp (Cyprinus carpio var. Jian). Animal Nutri 6:198–209